HHS Public Access

Author manuscript

Nano Lett. Author manuscript; available in PMC 2017 October 12.

Published in final edited form as:

Nano Lett. 2016 October 12; 16(10): 6661–6667. doi:10.1021/acs.nanolett.6b03470.

A Biocompatible and High Stiffness Nanophotonic Trap Array for Precise and Versatile Manipulation

Fan Ye[1,2,‡], **Ryan Badman**[1,‡], **James T. Inman**[1,2], **Mohammad Soltani**[1,2,3], **Jessica L. Killian**[1], and **Michelle D. Wang**[1,2,*]

[1]Department of Physics – LASSP, Cornell University, Ithaca, New York 14853

[2]Howard Hughes Medical Institute, Cornell University, Ithaca, New York 14853

Abstract

The advent of nanophotonic evanescent field trapping and transport platforms has permitted increasingly complex single molecule and single cell studies on-chip. Here, we present the next generation of nanophotonic Standing Wave Array Traps (nSWATs) representing a streamlined CMOS fabrication process and compact biocompatible design. These devices utilize silicon nitride (Si_3N_4) waveguides, operate with a bio-friendly 1064 nm laser, allow for several watts of input power with minimal absorption and heating, and are protected by an anticorrosive layer for sustained on-chip microelectronics in aqueous salt buffers. In addition, due to Si_3N_4's negligible nonlinear effects, these devices can generate high stiffness traps while resolving sub-nanometer displacements for each trapped particle. In contrast to traditional table-top counterparts, the stiffness of each trap in an nSWAT device scales linearly with input power and is independent of the number of trapping centers. Through a unique integration of micro-circuitry and photonics, the nSWAT can robustly trap, and controllably position, a large number of nanoparticles along the waveguide surface, operating in an all-optical, constant-force mode without need for active feedback. By reducing device fabrication cost, minimizing trapping laser specimen heating, increasing trapping force, and implementing commonly used trapping techniques, this new generation of nSWATs significantly advances the development of a high performance, low cost optical tweezers array laboratory on-chip.

Graphical Abstract

*Correspondence should be addressed to M.D.W. (mwang@physics.cornell.edu).

[3]**Present Address**

Raytheon BBN Technologies, Cambridge, MA 02138.

‡These authors contributed equally.

Author Contributions

The manuscript was written through contributions of all authors. All authors have given approval to the final version of the manuscript. F.Y. and R.B. designed and fabricated the devices. J.T.I., F.Y., and J.L.K. upgraded the nanophotonics measurement setup and F.Y. carried out measurements. M.S. obtained some preliminary data on some of the experiments. F.Y., R.B, and M.D.W. drafted the manuscript and all authors edited the manuscript. M.D.W. provided overall guidance on experimental designs and measurements.

Supporting Information. Fabrication protocol for Si_3N_4 nSWAT device, Data acquisition and analysis methods, Si_3N_4 waveguide loss measurement, microheater calibration curve, modulation speed measurement of the Ni microheater, 3D full-wave electromagnetic simulations, kymograph of long range transport of trapped bead array, stiffness measurements using three different methods, spatial resolution measurement of trap movement, cross-talk among different traps, and simultaneous trap stiffness calibration for an array of trapped beads. This material is available free of charge via the Internet at http://pubs.acs.org.

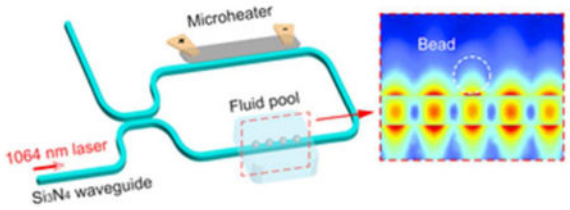

Keywords

optical trap; nanophotonics; array traps; standing wave; precise manipulation

Optical trapping utilizes the gradient forces of an electromagnetic field to trap and manipulate small dielectric particles.[1–9] A traditional free-space optical trap is a sensitive tool generated by a tightly focused laser beam using table-top optics. These traps can generate piconewtons (pN) of force and detect nanometer (nm) displacements[3, 5–9] and have become indispensable tools in physics, chemistry, and biology, and particularly in single molecule biophysics. Despite their significant utility, these large instruments are impeded by low throughput and an inherent susceptibility to environmental noise, and exceptional measures must be implemented to ensure their stability.[10–13] To increase throughput, holographic and time-sharing techniques have been used to generate tens to hundreds of traps in a single instrument, but this also requires increasing the laser power proportionally to the number of traps.[14–20]

An entirely different platform, driven by recent advances in nanophotonics, now permits on-chip trapping and transport via evanescent fields on nanophotonic waveguide surfaces (e.g. linear waveguide,[21, 22] resonator ring,[23] photonic crystal resonator,[24] and liquid core waveguides[25]). Compared with free-space optical traps, these nanophotonic platforms offer the advantage of scalability, as the same evanescent field can trap multiple particles, as well as potential for high stability due to the compact on-chip photonic designs. However, major challenges still face the application of nanophotonic traps for single biomolecule manipulation, namely in the realization of controllable, precision manipulation schemes for trapped objects at biologically-relevant ambient conditions and forces.

To deal with these challenges, we have recently developed a nanophotonic standing-wave array trap (nSWAT) that generates an array of traps at the antinodes of a standing-wave evanescent field of a nanophotonic silicon (Si) waveguide.[26] Representing the first nanophotonic device allowing controllable positioning of multiple, stably-trapped objects, the entire trap array can be precisely manipulated by thermo-optical modulation of the phase difference between two counter-propagating laser beams via an on-chip microheater.[27] Both nSWATs and previous free-space optical trapping using holographic/time-sharing methods allow the formation of a trapped array of tens to hundreds of traps. The advantage of the nSWATs is that it can do so without the need of increasing the laser power as the laser is recycled for multiple uses, although the trap spacing in an nSWAT cannot be readily varied and individually addressed, as would be possible for a trap array generated by holographic/time-sharing methods.

To make nSWAT devices more broadly accessible and biologically applicable, several measures are called for: a reduction in device fabrication cost, minimization of specimen heating by the trapping laser, an increase in trapping force, and implementation of various modes of operation commonly used in optical trapping. In this work, we achieve these features with a new generation of nSWATs enabling high-stiffness and long-range precision manipulation with increased modes of operation, most notably constant velocity[12, 28–42] and constant force,[12, 43–57] the two most commonly used manipulation schemes for single molecule studies. These critical abilities are novel in an on-chip environment and, when coupled with a streamlined, lower cost fabrication process results in an important milestone in creating a full optical tweezers array laboratory on-chip.

Fig. 1a shows a concept schematic of the core components of the new nSWAT devices. They were fabricated using deep-ultraviolet (DUV) lithography, versus the electron-beam lithography of the previous generation (Fig. 1; Supporting Information). This significantly reduces device cost and processing time, while retaining the high quality photonic performance typical of electron-beam lithography, as demonstrated by the smooth surfaces and straight side walls (Figs. 1b and 1c), and a measured waveguide propagation loss of 0.44 dB/cm (Fig. S1). Additionally, the previous generation Si waveguides are replaced by Si_3N_4 waveguides. Silicon nitride waveguides offer multiple practical advantages over silicon ones. They can operate with a laser of much shorter wavelength (e.g., 1064 nm used here versus 1550 nm used previously) with minimal non-linear absorption.[58, 59] These features not only reduce specimen heating by two orders of magnitude, but also permit an order of magnitude increase in laser power at the trapping region. These waveguides sustained up to 3W of input laser power (the limit of our current laser source) for high trap stiffness measurements without detectable damage, which is significantly more power tolerance than previously attainable with Si_3N_4 waveguides.[60] Finally, the microheaters, used to reposition the trap arrays via the thermo-optic effect (Fig. S2), were protected by an anticorrosive layer from the corrosive aqueous salt buffer and sustained voltage application of 10 volts over many tens of hours of experiments with no detectable corrosion in a 10 mM Tris (HCl) pH 8.0 buffer containing 100 mM NaCl.

The microheater also responds to the control voltage at a 30 kHz rate (Fig. S3), comparable to what is typically attainable by the AODs or piezo stages commonly used to steer a trap in bench-top optics.[29, 30] This speed is crucial for transport of an array of trapped beads over a long distance where the microheater's voltage must be rapidly reset to zero each time the trap array is transported by one spatial period λ_z of the standing-wave trapping potential before re-ramping the voltage.[26]

Such a method requires a precise knowledge of λ_z, which may differ somewhat from device to device. Here, we demonstrate a new method of phase tuning and its application in a constant speed mode. Using this phase tuning, the periodicity may be determined from just a single trapped bead, simplifying characterization while increasing precision. In this approach, a trapped bead is transported along the waveguide at a constant speed over a defined distance d by increasing the voltage before the voltage is reset and re-ramped. As shown in Figs. 2a–c, when $d = \lambda_z$, the bead moved forward seamlessly at the voltage resets. When $d > \lambda_z$, the bead position back-tracked along the waveguide at the voltage reset,

whereas when $d < \lambda_z$, the bead forward-tracked at the voltage reset. Thus, by minimizing the seams in the bead position at the voltage resets, the periodicity of the trapping potential can be precisely determined. Using this method, we found $\lambda_z = 360 \pm 5$ nm, which is in agreement with simulated results that give $\lambda_z = 355$ nm (Fig. S4). Once the periodicity is determined, the bead may be precisely moved at any constant or variable rate over a long distance along the waveguide. Fig. 2d shows an example of long distance transport in a constant velocity mode, where an array of trapped beads was smoothly moved along the waveguide at 3.6 μm/s over an 18 μm range before the direction was reversed (see also Fig. S5). Such an approach will enable manipulation of an array of biomolecules in a constant velocity mode.

Because the trap speed is modulated by the microheater voltage which can take a broad range of waveforms, nSWAT also allows the generation of user-specified variable velocity modes, such as sinusoidal velocity,[61] which is another mode of operation that has been exploited in optical trapping.

In many assays performed with traditional trapping platforms, it is important to maintain a constant force on the trapped object. This is typically achieved via active force feedback,[29] which, however, may introduce feedback noise in the force.[62] Current methods for all-optical constant force require either modifications of the trapping beam profile or limited bead motion in a trap.[63, 64] Here, we demonstrate that the nSWAT can readily operate in an all-optical, constant-force mode, without the need for any active feedback. Such a mode comes naturally out of the periodic feature of the trapping potential and is achieved when the array trap is moved more rapidly than a bead can respond to. This can be understood by considering the equation of motion for a bead in an array trap that is moved at a speed v_{trap}:

$$\beta \frac{dz}{dt} = F_{\max} \sin\left[\frac{2\pi}{\lambda_z}(z - v_{trap}t)\right] = F_{\max} \sin\left(\frac{2\pi z}{\lambda_z} - 2\pi f_{\text{trap}} t\right), \quad (1)$$

where z is the bead position along the waveguide, β the viscous drag coefficient for the bead, and $f_{\text{trap}} = v_{\text{trap}}/\lambda_z$ the equivalent frequency of the trap movement. This equation describes a damped-forced oscillator[65] at low Reynold's number, where the viscous drag force balances the optical force. Below a critical trap speed, $v_{\text{critical}} = F_{\max}/\beta$, or a critical trap movement frequency, $f_{\text{critical}} = F_{\max}/(\lambda_z \beta)$, the bead tracks the trap motion except for a force-dependent offset. Note that $f_{\text{critical}} = f_{\text{corner}}$ is the corner frequency of the Brownian motion of a bead held in a trap of a stationary array. However, above the critical trap speed, the bead can no longer fully track the trap motion. When $v_{\text{trap}} \gg v_{\text{critical}}$, the array trap effectively scans a quasi-stationary bead and the array trap exerts a constant force on the bead in the direction of trap motion:

$$F = \beta \left[v_{\text{trap}} - \sqrt{{v_{\text{trap}}}^2 - \left(\frac{F_{\max}}{\beta}\right)^2} \right] \quad (2)$$

This is a direct analogy to the passive torque wrench that we previously developed for the angular optical trap[32, 66] to exert a constant optical torque on a trapped particle without the need of any feedback.

Using this method, we show that when $v_{trap} \gg v_{critical}$, a trapped bead moved at a nearly constant speed with only a small, detectable drift from the expected baseline (Fig. 3a). The resulting mean-square-displacement (MSD) of the drift shows a linear dependence on time (Fig. 3b). These features are characteristic of a particle undergoing purely diffusive Brownian motion biased by a constant force. The diffusion constant measured in this way is, $D = k_B T/\beta = 4.1 \pm 0.1 \times 10^5$ nm^2/s, in agreement with that determined from the power spectrum analysis of a bead held in one of the traps of a stationary array: $D = 4.4 \pm 0.7 \times 10^5$ nm^2/s (Fig. S6). Using this diffusion coefficient, the optical force may be estimated from the viscous drag force (Fig. 3c). Although these results illustrate the diffusive motion of a free particle under a constant force, once the particle is attached to a biological system and becomes constrained, e.g., via a DNA molecule that is tethered to another surface,[38, 41] the Brownian motion of the particle will then be greatly suppressed by the biological molecule.

Fig. 3d shows the optical force as a function of trap speed and is in agreement with theoretical predictions. As expected, the measured critical speed increases linearly with the laser power. Furthermore, because a trapped bead can be moved in both directions, the quality of the standing wave may be directly assayed by the degree of anti-symmetry in the force versus trap speed relation. The highly anti-symmetric relation in Fig. 3a suggests an excellent standing-wave quality of the fabricated nSWAT, i.e., the 50/50 beam splitter has created two counter-propagating waves of essentially identical intensities.

Although both the constant velocity mode and the constant force mode are generated under a constant trap speed, the constant velocity mode is intended to operate below the critical trap frequency such that the particle and trap motions remain essentially in sync. In contrast, the constant force mode operates above the critical trap frequency, where the particle and trap motion are no longer in sync, and the particle, instead, experiences a constant force.

A distinctive feature of the nSWAT device is its built-in capacity for parallelized precision manipulation and measurements. We demonstrate here that this new generation of devices has achieved the benchmarks of a single, high-end precision optical trap, but in a high throughput fashion. To determine the spatial resolution of the trap movement, we generated square-wave steps of trap motion using the microheater and measured the response of bead motion. As shown in Fig. S7, 3.4-nm steps are readily detectable and 0.85-nm steps can be discerned. These data show that the spatial resolution of this current generation of nSWAT is comparable to that of benchtop optical traps typically used in singe molecule manipulation experiments.[12, 30, 36] However, while the nSWAT resolution is on par with traditional high-end optical tweezers, the nSWAT platform is inherently more noise-resistant than free space platforms due to the short optical path difference between the two counter-propagating trapping waves generated on chip.[26] Fig. 4a shows the measured positions of an array of beads in an nSWAT over time, demonstrating that an entire bead array can be stably trapped with minimal drift. In another example, while the positions of the trapped beads were monitored, an additional bead in the solution became trapped on the waveguide (Fig. S8).

However, the positions of the existing beads in the array showed no detectable changes (< 1 nm) upon this new addition, indicating minimal cross-talk among the trapped bead positions. This is due to the majority of the laser power (78%) being confined within the waveguide core (Fig. S4), making the waveguide mode insensitive to small perturbations around the waveguide. In addition to trap stability, this power confinement isolates the trapping region from the laser path and further reduces sample heating, another fundamental advantage of the nanophotonic waveguide platform compared with free-space traps.

To determine the force generation capacity, the trap stiffness values of an array of trapped beads were also simultaneously measured (Fig. 4a). We found a stiffness variation from bead to bead of about 5% (Fig. S9). The consistency in the trap stiffness along the waveguide is a further indicator of the quality and uniformity of the waveguide. It also indicates that the trapping power among all traps in the array was rather uniform. This was only possible because of the low loss waveguides (Figure S1) and minimal scattering by the trapping particles. Furthermore, we have compared trap stiffness using three different methods (Fig. 4b): the power spectrum method, the variance analysis method, as well as the critical trap movement frequency method described in this work. The latter methods also allows for a broader survey of the trapping quality and uniformity. The results from all three methods are in agreement. The trap stiffness of ~1 pN/nm per watt of power in the waveguide at the trapping region is of the same order of magnitude as that of a single conventional optical trap,[7, 36, 41, 67] while the same laser in an nSWAT is recycled to generate an entire array of traps, each with a comparable stiffness. For each trap in the array, the estimated maximum force $F_{max} = k_{trap} \lambda_z/(2\pi)$ is ~ 60 pN per watt. This, in combination with the high power tolerance of this new generation of the nSWAT, enables parallel high-stiffness trap array.

We have developed and characterized a significant new generation of nanophotonic trapping devices operating at a bio-compatible 1064 nm laser wavelength. An individual device contains an array of several hundred simultaneous, stable, and fully-positionable trapping centers, each with biologically relevant trapping force, negligible specimen heating, and efficient laser power use. Additionally, we have established the ability to readily switch between two useful modes of operation within the platform: constant velocity mode and constant force mode. These devices match or surpass current table-top laser traps in terms of sub-nm manipulation resolution, long-range manipulation ability, and scalability of the numbers of traps without loss of trap stiffness and maneuverability, all while yielding increased noise resistance and stability due to the short optical path length. Taken together, these features have made the Si_3N_4 nSWAT a compelling high-throughput, on-chip alternative to traditional free-space optical traps.

Acknowledgments

We thank Dr. Jun Lin and Summer Saraf for assistance in the preliminary work, as well as members of the Wang lab for a critical reading of the manuscript. We wish to acknowledge support from the National Institutes of Health under Ruth L. Kirschstein National Research Service Award (2T32GM008267) and National Science Foundation grant (MCB-1517764) to M.D.W., as well as the National Science Foundation Graduate Fellowships (DGE1144153 to R.B. and J.L.K.). This work was performed in part at the Cornell NanoScale Science and Technology Facility (CNF), a member of the National Nanotechnology Infrastructure Network, which is supported by NSF grant (ECCS-15420813), as well as in the Cornell Center for Materials Science Research (CCMR) Shared Facilities which are supported through the NSF MRSEC program (DMR-1120296).

References

1. Ashkin A, Dziedzic JM, Yamane T. Nature. 1987; 330(6150):769–771. [PubMed: 3320757]
2. Ashkin A, Dziedzic JM. Science. 1987; 235(4795):1517–1520. [PubMed: 3547653]
3. Svoboda K, Schmidt CF, Schnapp BJ, Block SM. Nature. 1993; 365(6448):721–727. [PubMed: 8413650]
4. Kuo SC, Sheetz MP. Science. 1993; 260(5105):232–234. [PubMed: 8469975]
5. Finer JT, Simmons RM, Spudich JA. Nature. 1994; 368(6467):113–119. [PubMed: 8139653]
6. Molloy JE, Burns JE, Kendrickjones J, Tregear RT, White DCS. Nature. 1995; 378(6553):209–212. [PubMed: 7477328]
7. Yin H, Wang MD, Svoboda K, Landick R, Block SM, Gelles J. Science. 1995; 270(5242):1653–1657. [PubMed: 7502073]
8. Smith SB, Cui YJ, Bustamante C. Science. 1996; 271(5250):795–799. [PubMed: 8628994]
9. Wang MD, Schnitzer MJ, Yin H, Landick R, Gelles J, Block SM. Science. 1998; 282(5390):902–907. [PubMed: 9794753]
10. Abbondanzieri EA, Greenleaf WJ, Shaevitz JW, Landick R, Block SM. Nature. 2005; 438(7067):460–465. [PubMed: 16284617]
11. Moffitt JR, Chemla YR, Izhaky D, Bustamante C. P Natl Acad Sci USA. 2006; 103(24):9006–9011.
12. Hall MA, Shundrovsky A, Bai L, Fulbright RM, Lis JT, Wang MD. Nat Struct Mol Biol. 2009; 16(2):124–129. [PubMed: 19136959]
13. Mahamdeh M, Schaffer E. Opt Express. 2009; 17(19):17190–17199. [PubMed: 19770938]
14. Dufresne ER, Grier DG. Rev Sci Instrum. 1998; 69(5):1974–1977.
15. Dufresne ER, Spalding GC, Dearing MT, Sheets SA, Grier DG. Rev Sci Instrum. 2001; 72(3):1810–1816.
16. Curtis JE, Koss BA, Grier DG. Opt Commun. 2002; 207(1–6):169–175.
17. Korda PT, Taylor MB, Grier DG. Phys Rev Lett. 2002; 89(12)
18. Curtis JE, Grier DG. Phys Rev Lett. 2003; 90(13)
19. Grier DG. Nature. 2003; 424(6950):810–816. [PubMed: 12917694]
20. van der Horst A, Forde NR. Opt Express. 2008; 16(25):20987–21003. [PubMed: 19065239]
21. Kawata S, Tani T. Opt Lett. 1996; 21(21):1768–1770. [PubMed: 19881795]
22. Yang AHJ, Moore SD, Schmidt BS, Klug M, Lipson M, Erickson D. Nature. 2009; 457(7225):71–75. [PubMed: 19122638]
23. Lin SY, Schonbrun E, Crozier K. Nano Lett. 2010; 10(7):2408–2411. [PubMed: 20545333]
24. Mandal S, Serey X, Erickson D. Nano Lett. 2010; 10(1):99–104. [PubMed: 19957918]
25. Kuhn S, Measor P, Lunt EJ, Phillips BS, Deamer DW, Hawkins AR, Schmidt H. Lab Chip. 2009; 9(15):2212–2216. [PubMed: 19606298]
26. Soltani M, Lin J, Forties RA, Inman JT, Saraf SN, Fulbright RM, Lipson M, Wang MD. Nat Nanotechnol. 2014; 9(6):448–452. [PubMed: 24776649]
27. Soltani M, Inman JT, Lipson M, Wang MD. Opt Express. 2012; 20(20):22314–22326. [PubMed: 23037380]
28. Baumann CG, Bloomfield VA, Smith SB, Bustamante C, Wang MD, Block SM. Biophys J. 2000; 78(4):1965–1978. [PubMed: 10733975]
29. Brower-Toland BD, Smith CL, Yeh RC, Lis JT, Peterson CL, Wang MD. P Natl Acad Sci USA. 2002; 99(4):1960–1965.
30. Koch SJ, Shundrovsky A, Jantzen BC, Wang MD. Biophys J. 2002; 83(2):1098–1105. [PubMed: 12124289]
31. Koch SJ, Wang MD. Phys Rev Lett. 2003; 91(2)
32. La Porta A, Wang MD. Phys Rev Lett. 2004; 92(19)
33. Brower-Toland B, Wacker DA, Fulbright RM, Lis JT, Kraus WL, Wang MD. J Mol Biol. 2005; 346(1):135–146. [PubMed: 15663933]

34. Jiang JJ, Bai L, Surtees JA, Gemici Z, Wang MD, Alani E. Mol Cell. 2005; 20(5):771–781. [PubMed: 16337600]
35. Shundrovsky A, Smith CL, Lis JT, Peterson CL, Wang MD. Nat Struct Mol Biol. 2006; 13(6):549–554. [PubMed: 16732285]
36. Deufel C, Wang MD. Biophys J. 2006; 90(2):657–667. [PubMed: 16258039]
37. Dechassa ML, Wyns K, Li M, Hall MA, Wang MD, Luger K. Nat Commun. 2011:2.
38. Ma J, Bai L, Wang MD. Science. 2013; 340(6140):1580–1583. [PubMed: 23812716]
39. Dame RT, Hall MA, Wang MD. Chembiochem. 2013; 14(15):1954–1957. [PubMed: 24000171]
40. Sheinin MY, Li M, Soltani M, Luger K, Wang MD. Nat Commun. 2013:4.
41. Inman JT, Smith BY, Hall MA, Forties RA, Jin J, Sethna JP, Wang MD. Nano Lett. 2014; 14(11): 6475–6480. [PubMed: 25291441]
42. Li M, Hada A, Sen P, Olufemi L, Hall MA, Smith BY, Forth S, McKnight JN, Patel A, Bowman GD, Bartholomew B, Wang MD. Elife. 2015:4.
43. Adelman K, La Porta A, Santangelo TJ, Lis JT, Roberts JW, Wang MD. P Natl Acad Sci USA. 2002; 99(21):13538–13543.
44. Adelman K, Yuzenkova J, La Porta A, Zenkin N, Lee J, Lis JT, Borukhov S, Wang MD, Severinov K. Mol Cell. 2004; 14(6):753–762. [PubMed: 15200953]
45. Brower-Toland B, Wang MD. Method Enzymol. 2004; 376:62–72.
46. Shundrovsky A, Santangelo TJ, Roberts JW, Wang MD. Biophys J. 2004; 87(6):3945–3953. [PubMed: 15465875]
47. Bai L, Fulbright RM, Wang MD. Phys Rev Lett. 2007; 98(6)
48. Deufel C, Forth S, Simmons CR, Dejgosha S, Wang MD. Nat Methods. 2007; 4(3):223–225. [PubMed: 17322891]
49. Johnson DS, Bai L, Smith BY, Patel SS, Wang MD. Cell. 2007; 129(7):1299–1309. [PubMed: 17604719]
50. Forth S, Deufel C, Sheinin MY, Daniels B, Sethna JP, Wang MD. Phys Rev Lett. 2008; 100(14)
51. Sheinin MY, Wang MD. Phys Chem Chem Phys. 2009; 11(24):4800–4803. [PubMed: 19506753]
52. Daniels BC, Forth S, Sheinin MY, Wang MD, Sethna JP. Phys Rev E. 2009; 80(4)
53. Patel G, Johnson DS, Sun B, Pandey M, Yu X, Egelman EH, Wang MD, Patel SS. J Biol Chem. 2011; 286(23):20490–20499. [PubMed: 21515672]
54. Forth S, Deufel C, Patel SS, Wang MD. Biophys J. 2011; 101(2):L5–L7. [PubMed: 21767475]
55. Sheinin MY, Forth S, Marko JF, Wang MD. Phys Rev Lett. 2011; 107(10)
56. Sun B, Johnson DS, Patel G, Smith BY, Pandey M, Patel SS, Wang MD. Nature. 2011; 478(7367): 132–U148. [PubMed: 21927003]
57. Sun B, Pandey M, Inman JT, Yang Y, Kashlev M, Patel SS, Wang MD. Nat Commun. 2015:6.
58. Dinu M, Quochi F, Garcia H. Appl Phys Lett. 2003; 82(18):2954–2956.
59. Ikeda K, Saperstein RE, Alic N, Fainman Y. Opt Express. 2008; 16(17):12987–12994. [PubMed: 18711537]
60. Ahluwalia BS, Subramanian AZ, Helleso OG, Perney NMB, Sessions NP, Wilkinson JS. Ieee Photonic Tech L. 2009; 21(19):1408–1410.
61. Svoboda K, Block SM. Cell. 1994; 77(5):773–784. [PubMed: 8205624]
62. Elms PJ, Chodera JD, Bustamante CJ, Marqusee S. Biophys J. 2012; 103(7):1490–1499. [PubMed: 23062341]
63. Greenleaf WJ, Woodside MT, Abbondanzieri EA, Block SM. Phys Rev Lett. 2005; 95(20)
64. Nambiar R, Gajraj A, Meiners JC. Biophys J. 2004; 87(3):1972–1980. [PubMed: 15345573]
65. Strogatz, SH. Nonlinear dynamics and Chaos: with applications to physics, biology, chemistry, and engineering. Addison-Wesley Pub; Reading, Mass: 1994. p. xip. 498
66. Inman J, Forth S, Wang MD. Opt Lett. 2010; 35(17):2949–2951. [PubMed: 20808379]
67. Wang MD, Yin H, Landick R, Gelles J, Block SM. Biophys J. 1997; 72(3):1335–1346. [PubMed: 9138579]

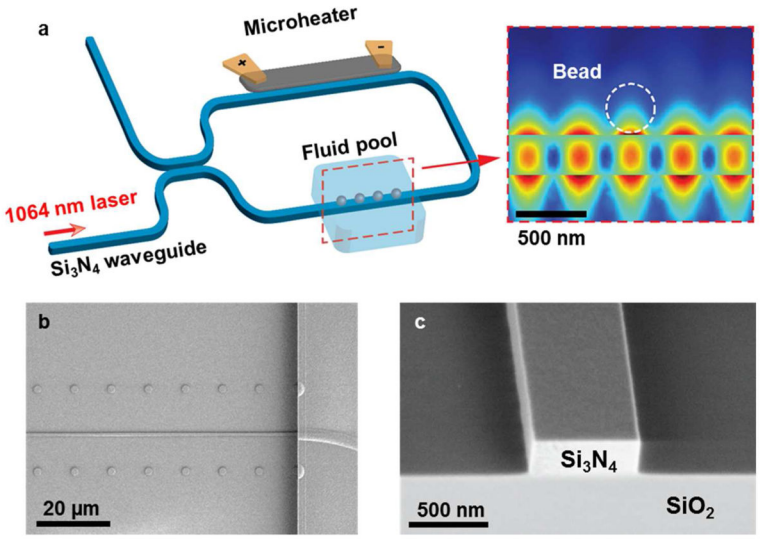

Figure 1.

Si_3N_4 nSWAT design and characterization. (a) A schematic of the core components of a Si_3N_4 nSWAT device. A 1064 nm laser is coupled into the TM mode of a Si_3N_4 waveguide through a tapered single mode fiber. After the laser passes through a 50/50 splitter, two counter-propagating waves form a standing-wave in the loop where a fluid pool region for trapping is also located. The standing-wave creates a periodic trapping potential along the waveguide, with the periodicity being the spacing between two adjacent anti-nodes. A microheater modulates the phase of one counter-propagating wave relative to the other via the thermo-optic effect, and thus repositions the trap array in response to an applied voltage. Inset to the right is a cross-section of the electric field profile from a 3D full-wave electromagnetic simulation in the presence of a 349 nm polystyrene bead trapped at one of the anti-nodes of the standing-wave formed along the Si_3N_4 waveguide. Color scale from blue to red is 0 to 7×10^7 V/m, respectively. (b) A SEM micrograph of the top view of the fluid pool region of a Si_3N_4 device. The fluid pool is etched down to expose the Si_3N_4 waveguide for bead trapping. Small circles are fiducial markers used for position tracking. (c) A SEM micrograph of the cross-section of a fabricated Si_3N_4 waveguide. The waveguide has a cross-section of 660 nm in width and 250 nm in height.

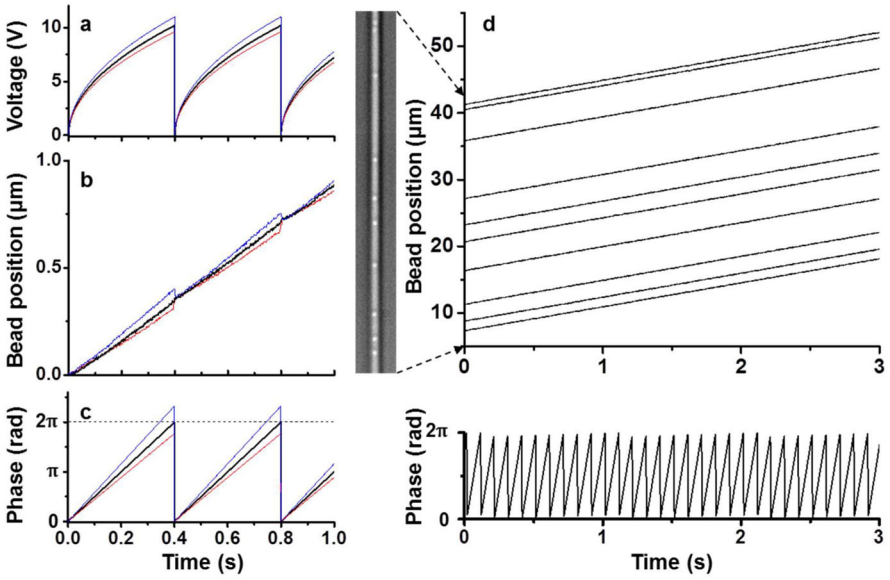

Figure 2.

Phase-tuning for long distance transport. (a) Periodic waveform of the voltage applied to the microheater for transport. Three different voltage amplitudes are shown. (b) The corresponding measured position of a trapped bead along the waveguide, in response to (a). (c) The corresponding phase change in the standing wave. (d) An example of a long-range transport of an array of trapped beads. The top plot shows positions of a trapped bead array versus time, with an image of the initially trapped bead array shown to the left. The bottom plot shows the corresponding phase change introduced by the microheater. Measurements were conducted at 16.6 mW of laser in the trapping region.

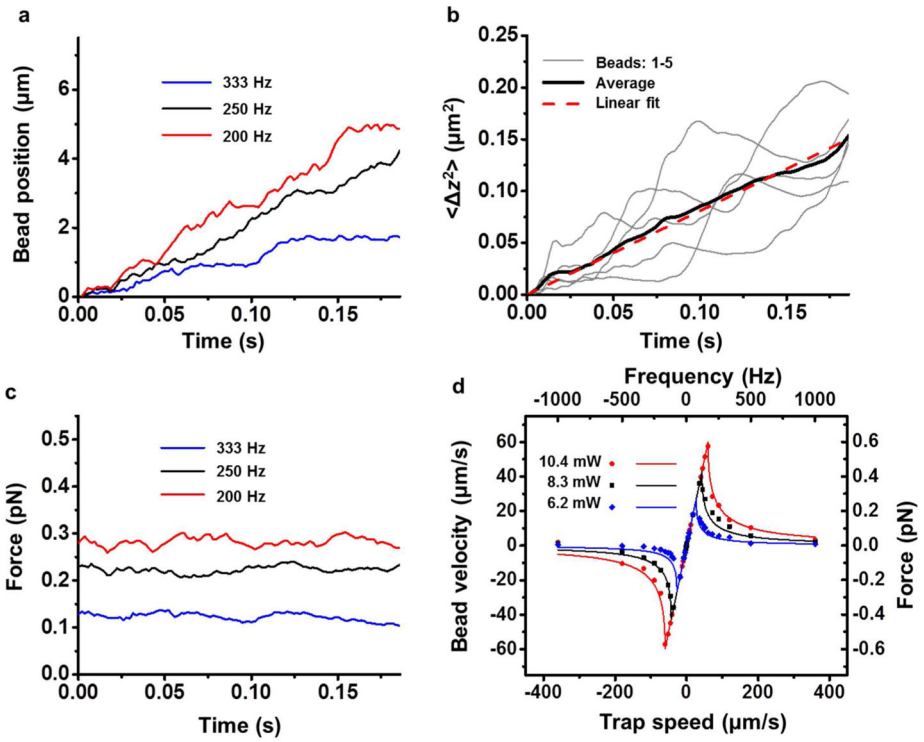

Figure 3.

All optical constant force mode. (a) The motion of a trapped bead under the constant force mode. Under 10.4 mW of laser power in the trapping region (corresponding to a critical frequency of 166 Hz), a trapped bead was moved in the forward direction along the waveguide under three different trap movement frequencies. (b) Mean squared displacement (MSD) from the linear drift. Experiments were conducted with five different trapped beads (five grey curves) at the 250 Hz trap movement frequency. Each trace of bead position versus time plot was fit by a line which represents the drift due to the force. The mean-square-displacement from this fit was then computed. The average MSD from these traces (solid black) was fit to a line (red) to obtain the one-dimensional diffusion coefficient ($4.1 \pm 0.1 \times 10^5$ nm^2/s). Viscous drag force was determined based on the bead speed and the measured diffusion coefficient. (c) The corresponding viscous drag force on the bead from (a). Viscous drag force was obtained as a cumulative moving average of the bead speed. (d) Trapped bead speed and corresponding viscous drag force versus trap speed and corresponding trap movement frequency. Data were taken under three different laser powers. Dots indicate measurements and solid curves are fits to Eq. (2).

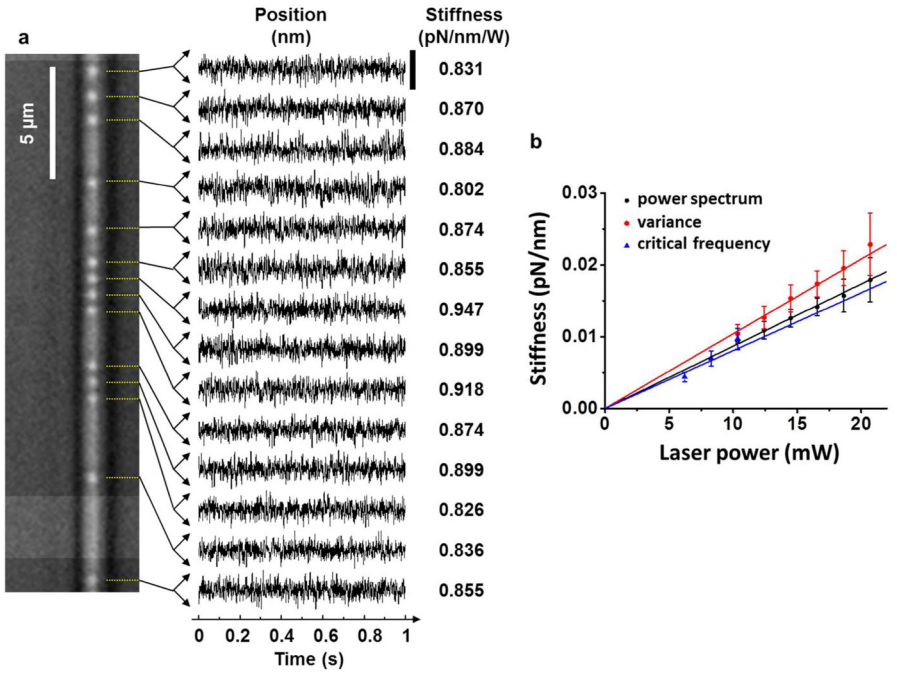

Figure 4.

Parallel precision measurements. (a) An array of beads was trapped on the waveguide and their positions were monitored over time. The middle panel provides a zoomed in view of the position of each bead versus time, with its stiffness per watt of laser power at the trapping region shown to the right. The images were acquired at 540 Hz. The black scale bar corresponds to 100 nm. (b) Trap stiffness measurements using three different methods: the power spectrum method, the variance method, and the critical frequency method described in this work. The linear fits for the three methods are: 1.01 pN/nm/W for the variance analysis method, 0.87 pN/nm/W for the power spectrum method, and 0.82 pN/nm/W for the critical trap movement frequency method. Error bars are standard errors of the means.